Host-parasite fluctuating selection in the absence of specificity

Alex Best[1*], Ben Ashby[2,3], Andy White[4], Roger Bowers[5], Angus Buckling[6], Britt Koskella[3] and Mike Boots[3,6]

[1]*School of Mathematics & Statistics, University of Sheffield, Sheffield, S3 7RH, UK.*

[2]*Department of Mathematical Sciences, University of Bath, Claverton Down, Bath, BA2 7AY, UK.*

[3]*Department of Integrative Biology, University of California Berkeley, Berkeley, CA, USA.*

[4]*Department of Mathematics and the Maxwell Institute for Mathematical Sciences, Heriot-Watt University, Edinburgh, EH14 4AS, Scotland, UK.*

[5]*Department of Mathematical Sciences, Division of Applied Mathematics, Mathematical Sciences Building, The University of Liverpool, L69 7ZL, UK.*

[6]*Biosciences, College of Life and Environmental Sciences, University of Exeter, Cornwall Campus, Treliever Road, Penryn, Cornwall, TR10 9EZ, UK.*

** Corresponding author*

Running Head: Cycles in host-parasite coevolution

Abstract

Fluctuating selection driven by coevolution between hosts and parasites is important for the generation of host and parasite diversity across space and time. Theory has focused primarily on infection genetics, with highly specific 'matching allele' frameworks more likely to generate fluctuating selection dynamics (FSD) than 'gene-for-gene' (generalist-specialist) frameworks. However, the environment, ecological feedbacks, and life-history characteristics may all play a role in determining when FSD occurs. Here, we develop eco-evolutionary models with explicit ecological dynamics to explore the ecological, epidemiological and host life-history drivers of FSD. Our key result is to demonstrate for the first time that specificity between hosts and parasites is not required to generate FSD. Furthermore, highly specific host-parasite interactions produce unstable, less robust stochastic fluctuations in contrast to interactions that lack specificity altogether or those that vary from generalist to specialist, which produce predictable limit cycles. Given the ubiquity of ecological feedbacks and the variation in the nature of specificity in host parasite interactions, our work emphasizes the underestimated potential for host-parasite coevolution to generate fluctuating selection.

Key Words

Coevolution, infectious disease, fluctuating selection, specificity

Introduction

Understanding the coevolution of hosts and parasites is important given the central role that infectious disease plays in human health, agriculture and natural systems. Theory predicts that the coevolution of hosts and their parasites may lead to a number of distinct outcomes, including a co-evolutionary stable strategy (co-ESS) for both host and parasite [1,2]; static within population dimorphism or polymorphism [2-5]; escalation (known as arms race dynamics, ARD) [6]; and fluctuating selection dynamics (FSD) [7-11]. Arms race dynamics cannot continue indefinitely due to associated fitness costs or physiological constraints (e.g. [12]), which means that, in the long term, coevolution will eventually lead to either a stable evolutionary equilibrium (including polymorphisms) or fluctuating selection. Fluctuating selection is therefore of particular importance because it is the only dynamic coevolutionary outcome that can be maintained indefinitely in a constant environment. The presence of a constantly changing antagonist is thought to play a key role in the maintenance of diversity [13], and also has implications for selection for sex and recombination [14-16], and local adaptation [17-19]. Understanding the processes and mechanisms that promote FSD therefore has significant implications for our understanding of a wide range of biological phenomena.

Theoretical work has primarily focused on how different forms of genetic specificity between hosts and parasites lead to fluctuating selection [7-11;19-21]. Highly specific 'matching allele' interactions, where parasites must 'match' the host at each loci to infect, commonly generate coevolutionary 'cycles' (i.e. FSD) as

selection favors parasite genotypes capable of infecting common host genotypes, thereby generating negative frequency-dependent selection [20-22]. Effectively, hosts constantly evolve to 'escape' parasites that can infect them while parasites play 'catch-up'. In contrast, 'gene-for-gene' interactions (where there is variation in specificity such that hosts and parasites vary from specialists to generalists) often produce arms race dynamics (ARD), where directional selection favors increasing resistance and infectivity ranges, although there can be a transition to FSD if there are costs to infection and defense [7-11]. While some empirical evidence appears consistent with the notion that different genetic interactions are associated with ARD or FSD [23-25], recent experimental work has shown that changing environmental conditions can cause host-parasite interactions to switch between ARD and FSD [26-28], suggesting either that the environment determines specificity or that the same genetic specificity has different consequences depending on the environment.

One way to investigate the importance of genetic specificity alongside ecological feedbacks in determining FSD is to directly compare coevolutionary dynamics with no specificity with those generated under various different forms of specificity. This can be achieved using eco-evolutionary models, which allow for varying population sizes due to changes in host defence and parasite infectivity. These models are increasingly used to examine the role of environmental and ecological feedbacks on the coevolution of hosts and parasites [1,2,4,5,29] and have largely considered the processes that determine co-ESS levels of host defense and parasite infectivity, and the potential for diversification through evolutionary branching. For example, it has been shown that the likelihood of static, within-

population diversification depends on the nature of host-parasite genetic specificity, associated fitness costs, and explicit ecological dynamics [5]. The form of the infection interaction was crucial to the level of diversity that could arise, with non-specific 'universal' functions (parasite A always has higher transmission than parasite B against any host) leading to dimorphism at most, but 'range' functions with variation in specificity (whereby the relative success of parasite strains depends on the target host) potentially leading to higher levels of polymorphism [5]. This work emphasized the important role that ecological feedbacks play in host-parasite coevolution. Little of this work, however, has considered the potential for fluctuating selection [4,27] and none has provided a full exploration of the ecological, epidemiological and host life-history drivers of FSD.

Here we examine how host and parasite life-history characteristics and the specificity of their interaction, in combination with ecological feedbacks, determine the likelihood of fluctuating selection. By 'specificity', we mean the degree to which parasite strains specialise on a subset of host types. An interaction is defined to be 'specific' if each parasite strain has higher transmission against some hosts and lower transmission against others compared to another parasite strain. Conversely, an interaction is 'non-specific' if each parasite strain always has either higher or lower transmission against all hosts compared to another parasite strain. We consider interactions between hosts and parasites starting from 'universal' (all non-specific), to 'range' (variation from highly specific to generalist, and therefore phenotypically equivalent to gene-for-gene models but with continuous phenotypic variation), and 'matching' (highly specific, where all

parasite strains are specialists on respective host strains, and therefore phenotypically equivalent to matching allele models but again with continuous phenotypic variation). Furthermore we explicitly consider the ecological and epidemiological settings that promote cycles. As such we determine what factors and which types of host-parasite interactions promote fluctuating selection.

Model and Methods

We base our mathematical analysis within the eco-evolutionary invasion framework known as adaptive dynamics [30-33] and combine this with explicit evolutionary simulations that relax some of the restrictive assumptions of the mathematical approach (see §A1 in SI for a fuller description of the analytic methods, and §B for a description of the numerical simulations). We assume that resident strains of host and parasite have reached a population dynamic equilibrium of a Susceptible – Infected – Susceptible model [5,34],

(1) $\frac{dS}{dt} = (a - q(S + I))(S + fI) - bS - \beta SI + \gamma I$

(2) $\frac{dI}{dt} = \beta SI - (b + \alpha + \gamma)I$.

Susceptible hosts reproduce at rate a, with the rate for infected hosts reduced by $f \in [0,1]$, with reproduction limited by competition by a density-dependent factor q. All hosts die at natural mortality rate b, but infected hosts suffer an additional mortality at rate α, which we define as 'virulence' (in contrast to the plant-pathogen literature where virulence is often defined as infectivity). Transmission

is assumed to be a mass action density-dependent interaction with coefficient β. We assume that both the host and parasite have some 'control' over the transmission rate, so that transmission is dependent on the host trait, h, and parasite trait p, with $\beta = \beta(h, p)$. We will generally define h as susceptibility (I.e., inversely, resistance) and p as infectivity. Finally hosts can recover from infection at rate γ. For our algebraic analysis we will make the simplifying assumptions that $\gamma = 0$ and $f = 0$, but we shall relax these assumptions in our numerical investigations.

We assume that a resident host (h) and parasite (p) are at their endemic steady state and that a rare mutant strain of either the host ($\bar{h}$; overbars denoting mutant traits) or parasite ($\bar{p}$) attempts to invade (with trait values limited to $h \in [0,1]$ and $p \in [0,1]$ by some physiological constraints). The mutant has small phenotypic differences to the current resident strain and therefore a different transmission coefficient. We assume trade-offs in which a decrease in transmission (either an absolute reduction or an increase in resistance range; see below) caused by a host mutation confers a cost to the host birth rate, $a(h)$, while an increase in the base transmission rate caused by a parasite mutation confers either an increase in virulence, $\alpha(p)$, or a reduced infection range [4,5]. The success of the mutant depends on its invasion fitness when the resident is at its ecological equilibrium. In the simplified case where $\gamma = 0, f = 0$ (see SI §A1 for general case), the respective host and parasite fitnesses are,

(3) $s(\bar{h}; h, p) = a(\bar{h}) - q(\hat{S} + \hat{I}) - b - \beta(\bar{h}, p)\hat{I}$,

(4) $r(\bar{p}; h, p) = \beta(h, \bar{p})\hat{S} - b - \alpha(\bar{p})$

(where hats denote equilibrium densities of the resident). If a mutant has positive invasion fitness it will invade to replace or coexist with the current resident (subject to demographic stochasticity [30]), while if it has negative fitness it will die out. Through a series of mutations and substitutions the two species will coevolve in the directions of their local selection gradients, with the canonical equations [30,31] given by

$$(5)\ \frac{dh}{dt} = \varphi^h \hat{S} \frac{\partial s}{\partial \bar{h}}\Big|_{\bar{h}=h} = \varphi^h \hat{S}[a_{\bar{h}} - \beta_{\bar{h}}\hat{I}]$$

$$(6)\ \frac{dp}{dt} = \varphi^p \hat{I} \frac{\partial r}{\partial \bar{p}}\Big|_{\bar{p}=p} = \varphi^p \hat{I}[\beta_{\bar{p}}\hat{S} - \alpha_{\bar{p}}]$$

where subscripts denote derivatives (i.e. $\beta_{\bar{h}} = \partial\beta(\bar{h}, p)/\partial\bar{h}$) and φ^i controls the respective speeds of mutation (which are products of the mutation rate and variance and a factor of 1/2). To simplify what follows we shall set $\varphi^h = \varphi^p = 1$. Note that all the derivatives are evaluated at the resident trait values, $\bar{h} = h, \bar{p} = p$.

A coevolutionary 'singular point' is a point at which the two selection gradients are simultaneously zero (i.e. there is no longer directional selection on either species). There are four behaviors at a singular point that are of particular interest. First, the singular point can be a long-term attractor of evolution (*Continuously Stable Strategy* or CSS; a dynamic counterpart to the classic Evolutionarily Stable Strategy (ESS)). Second, the singular point can be an *evolutionary branching point* for that species. Here one of the species will undergo disruptive selection and

branch into two coexisting strains. Third, if varying parameter values causes the system to pass a critical point (a Hopf bifurcation [36]) then *coevolutionary cycles* will result (although further work is required to find whether the resulting cycles are stable, resulting in FSD, or unstable, resulting in bistability). Finally, a repelling singular point could cause directional selection in the host and/or parasite to *maximize or minimize* their investment to bounds of evolution (recall $h, p \in [0,1]$), while the other species may reach a purely evolutionary CSS (i.e. a host CSS may exist where *p=1*), may branch or may also maximize/minimize.

It is clearly important to examine the precise nature of the infection function, $\beta(h,p)$, to determine coevolutionary dynamics. Following previous work [5], here we use three key functional forms: 'universal' (no specificity), 'range' (variation from specialism to generalism), and 'matching' (highly specific). These are shown as heat maps in figure 1, where red denotes high transmission rates for combinations of *h* and *p* and blue low transmission. In detail:

The universal function is given by,

(7) $\beta(h,p) = \sigma(h)\rho(p) + k,$

where *k* is a constant giving the minimum value of the infection function. In this case there is no specificity, as figure 1a highlights that parasites retain the same relative ordering of infection rates against any host (see also fig S1a in the SI). As such, each host is 'universally' more resistant moving from right-to-left (here $\beta_h >$

0, where the subscript denotes differentiation with respect to h) and similarly for parasites (b_p >0).

The range function is given by,

(8) $\beta(h,p) = \beta_0(p)\left(1 - \frac{1}{1+\exp(\kappa(p-h))}\right)$,

where κ is a constant controlling the steepness of the curve. In this case there is variation in specificity, representing hosts and parasites that range from specialist to generalist. A parasite trade-off, $\beta_0(p)$, is built in to the infection function so that parasites with a narrow range (low p) achieve higher transmission against the least resistant hosts (the cost of a large range is thus a low transmission rate, and we assume no further parasite trade-offs to virulence; including an additional virulence trade-off has no qualitative impact on the results presented here). The range function, as shown in figure 1b (see also fig S1b) therefore includes specificity as for low h parasites with low p have the highest transmission, but for high h parasites with high p are the most infectious. Hence, parasites vary in the range of hosts that they can successfully infect, and similarly for host resistance.

For the matching function,

(9) $\beta(h,p) = \beta_0(p)exp\left(-\left(\frac{p-h}{\eta p+c}\right)^2\right)$,

where η and c are constants controlling the variance of the infection curves. Here a 'match' between host and parasite strains is required for optimal infection, with the transmission rate falling away as they become more distant. This function therefore corresponds to a high degree of specificity between host and parasite. The case where η=0 and $\beta_0(p)$ is constant (i.e. there are no costs to the parasite) represents a continuous analogy of matching alleles infection genetics, as shown in figure 1c (see also fig S1c; e.g. [5]). When η>0 and we assume costs, the trade-off ensures that parasites with a narrow range achieve higher transmission against their matching hosts relative to parasites with a broader range (again, there is no virulence trade-off in the matching model), as shown in figure 1d (see also fig S1d). This is in some sense a hybrid matching-range function, but the maximum transmission of a parasite is not always against the least resistant hosts (compare figs 1b and 1d).

Results

Specificity of the infection function

In the SI §A2 we show that if there are no fitness costs to host resistance or parasite infectivity, then a coevolutionary singular point can never exist for the universal or range functions. Since selection now only acts on transmission the host will always evolve to minimize investment and the parasite to maximise (to bounds of evolution). For the matching function with no costs (i.e. figure 1c), there will be a continuum of singular points at $h=p$ none of which are attracting. Under the full assumptions of adaptive dynamics, this will lead to a random walk through trait space. However, if we relax the assumption of mutations occurring rarely,

fluctuating selection occurs due to the 'trail' of strains on one side of the current resident. This build up of strains keeps the host or parasite evolving in the same direction for longer, with reversals in selection due to one antagonist 'passing' the other becoming more rare. We term these '*stochastic oscillations*', since they are non-deterministic, unstable cycles whose existence depends on the discrete and stochastic assumptions of the simulations. An example of these stochastic oscillations can be found in [5]. For the remainder of this study we assume that host resistance and parasite infectivity are costly.

We initially consider whether coevolutionary cycles can ever emerge for each infection function. This is particularly important for the universal function since cycles in this model have never been demonstrated (see [4] and [27] for examples of cycles in the range model). To achieve this, initially we simply wish to show that parameters and trade-offs exist that produce a Hopf bifurcation, using a method previously employed to find cycles between parasite virulence and predator population densities [36]. The full analysis is given in the SI §A2.

In the universal model (7) cycles will be possible (for some parameters and trade-offs) wherever $k > 0$. However, there is a special case for $k=0$ (i.e. the minimum value of the infection function is 0), where we show there can never be cycles (see SI §A2i). Biologically, this means that cycles in quantitative levels of resistance and infectivity will not occur unless parasites have a non-zero baseline level of transmission, and is due to the host trait having no impact on parasite selection in this special case (see SI §A2i). This explains why in a previous study we found no evidence of coevolutionary cycles with the universal transmission function

$\beta(h,p) = hp$ [2]. Figure 2a shows numerical simulations of the coevolutionary dynamics for the case where $\beta(h,p) = hp + 0.5$ (i.e. $k > 0$) with regular coevolutionary cycles. These cycles lead to regular increases and decreases in quantitative host resistance and parasite infectivity (transmission) and virulence. The cycles arise simply due to the negative frequency dependence resulting from the epidemiological feedbacks on disease prevalence from the evolution of resistance and infectivity.

We find that a Hopf bifurcation may occur for any form of the range infection function (8). The cycles that emerge will be in the respective resistance and infection ranges of hosts and parasites, as demonstrated previously [4,27]. Figure 2b shows the output from simulations of the coevolutionary dynamics, once again showing regular cycles.

Assuming costs in the matching model (9) we again find that a Hopf bifurcation may always occur. However, in this case numerical analysis of the system indicated that the Hopf bifurcation is always *subcritical*, meaning that the cycles are unstable (i.e. not attracting) [35,36]. We explored a comprehensive range of parameter sets and trade-offs but saw no examples of stable coevolutionary cycles in bifurcation diagrams or numerical simulations. Instead there is generally a bistability such that, under the full assumptions of adaptive dynamics, the system should evolve either to an intermediate singular point or to a minimum. However, as is the case when there were no costs, when the assumptions are relaxed in numerical simulations we typically see fluctuating selection. An example of these dynamics are shown in figure 2c where we see rather irregular oscillations. These

are once more non-deterministic, stochastic oscillations. Such stochastic effects are inherent in natural systems and therefore these oscillations are likely to occur in nature, but we emphasize that these are less regular and predictable than those seen for the universal and range models (c.f. figures 2a,b). Why do such oscillations emerge? In general the host will always evolve away from the parasite and the parasite will evolve to match the host, leading to a 'chase' across phenotypic space (which is again linked to the presence of the 'trail' of strains present when mutations are not strictly rare). However, we found that provided the trade-offs are not too strongly decelerating or accelerating, the h and p nullclines generally remain very close to the main diagonal ($h=p$) meaning that a small mutation can easily cross the nullclines and reverse the direction of selection, causing the 'chase' to go in the other direction (see figure S6 in the SI). These repeated crossings of the nullcline by small, finite mutations are what drive the oscillations.

Host and parasite life-history characteristics

We now explicitly consider the ecological conditions that favour FSD by varying host and parasite life-history traits for each infection function. For the stable cycles we do this by computing bifurcation diagrams using the numerical continuation software AUTO-07p [37]. For the stochastic oscillations we examine numerical simulations. In each case we shall explore the effects of altering (a) resource competition, q, and (b) the virulence, a. Plots for the other parameters (b, g and f) can be found in figures S2, S3 and S5 in the SI.

The behavior in the universal model as resource competition, q, is varied is representative of all of the bifurcation diagrams (figure 3a, S2). The red vertical dashed lines in figure 3 separate the regions of behavior, as annotated along the bottom. Starting from the right-hand end of figure 3a, the trend as q is decreased is: no singular point, leading to minimization; the emergence of a pair of singular points through a saddle-node bifurcation (solid line: a branching point, dashed line: a repeller) often leading to branching; a Hopf bifurcation leading to the onset of cycles which increase in size (solid grey line marks the maximum and minimum values reached on a cycle); the loss of cycles such that both host and parasite maximize (i.e. ARD). We see similar behavior in figure 3b as virulence is varied (although here the saddle-node bifurcation occurs for rates of virulence beyond the domain of this plot). Decreasing values of q and α lead to increased densities of infectious individuals, and hence higher encounter rates with susceptible hosts. It is interesting to note that "static diversity" (branching to coexistence) occurs for lower encounter rates than "temporal diversity" (FSD). We conclude that FSD will be promoted in intermediate/large sized populations (intermediate q, low b, intermediate f) with an intermediate infectious period (intermediate a, low b, intermediate g). In §A3 and figure S5 in the SI we also show that cycles occur for a range of weakly decelerating trade-offs in both the host and parasite.

The bifurcation plots for the range model in figures 3c,d show very similar behavior to those for the universal model (figures 3a,b), except that a new behavior emerges with regions where the singular point is an attracting *Continuously Stable Strategy* (CSS). The conditions that promote FSD in the range model are qualitatively similar to those in the universal model.

To explore the effects of life-history characteristics on the stochastic oscillations in the matching model we ran evolutionary simulations and measured the variance in the host trait over the final 20% of each run. A higher variance indicates larger stochastic oscillations (the values where there is zero variance actually relate to parasite extinction). In figure 4 (figure S3 in the SI) we see a similar pattern to the above results – the variance is greatest in long-lived (low b), large populations (low q, low b) with high infectious periods (low α, low γ, low b).

Discussion

We have analyzed a series of host-parasite coevolutionary models to understand how ecological dynamics, life-history characteristics, and the specificity of interactions between hosts and parasites impact fluctuating selection dynamics (FSD). A key finding is that FSD in host resistance and parasite infectivity may occur without the need for any specificity in the interaction between hosts and parasites. When there is specificity, we find that the nature of fluctuating selection is very different in a highly specific matching interaction (akin to matching alleles in that all parasite strains are specialists on respective host strains) compared to when there is variation in the range of specificity (akin to gene-for-gene in that there is variation in specificity such that hosts and parasites vary from specialists to generalists). Therefore, although it is already known that both types of specific infection mechanism can lead to FSD, our models suggest that the nature of the underlying fluctuations are fundamentally different [see also 9]. Finally, we show

how both host and parasite characteristics influence the likelihood of fluctuating selection, which allows us to predict the ecological conditions that are most likely to show FSD. This is important because it tells us when fluctuating selection is likely to generate genetic diversity through time [13].

The fact that fluctuating selection can arise without specificity between hosts and parasites is of particular interest because much theoretical and empirical work has focused on identifying the relationship between different types of specificity and FSD rather than considering the potential for FSD in non-specific interactions [7-11; 23-25]. We have shown that costs associated with non-specific resistance and infectivity can be sufficient to generate coevolutionary cycles in an eco-evolutionary setting. In principle, these cycles would also be possible in a non-ecological framework where selection is frequency-dependent but not density-dependent, as one could choose fitness functions whereby the selection gradients are never simultaneously zero on a closed trajectory. However, it is realistic to assume that the relative population densities, and thus the prevalence of infection, will vary with changes in host resistance and parasite infectivity. The feedbacks generated by these changes provide a natural route for frequency-dependent selection to operate and generate fluctuations. The drivers of the cycles in both the universal and range models are thus due to a mix of frequency-dependence (i.e. relative infection rates) and density-dependence (i.e. varying population sizes due to ecological feedbacks). Cycles without specificity have not been described previously, as most studies on FSD have neglected ecological dynamics and feedbacks. Those evolutionary studies that do include ecology have either assumed specificity between host and parasite and not examined universal

interactions [16, 38-44], or, have assumed universal infection but focused on optimal investment or evolutionary branching rather than cycling [1-5; 29]. Our work examines models with explicit ecological dynamics and focuses on the potential for FSD both with and without specificity.

Ecology has been shown to drive fluctuating selection in predator-prey systems with specificity [31,45] (although we note that the `matching' function considered in these studies is different from the one used here). However, our work shows that it also occurs in non-specific host-parasite interactions. This result has important relevance to the role host-parasite coevolution may play in shaping host diversity across space and time. When host fitness depends on the frequency of different parasite genotypes, there are predicted to be differences among populations in terms of which host and parasite genotypes are being selected for at a given point in time. Hence, the propensity for fluctuating selection will have impacts on host–parasite local adaptation, as isolated populations are likely to be out of sync with one another [19,46]. There are also implications to the theory surrounding the evolution of sexual reproduction. While evolution of sex studies typically take a population genetics approach with a few major loci, it has been shown that sex can be beneficial where there are many loci with small additive effects [47]. One common criticism of the Red Queen hypothesis for the maintenance of sex is the lack of highly specific and virulent parasites that are generally assumed to be necessary for FSD [48]. Our work suggests these restrictive assumptions could be relaxed; future theory must test whether selection for sex can be generated in the absence of specificity and for parasites with only intermediate levels of virulence.

While we found that FSD could occur across all of the interactions we considered, we found that the nature of the cycles are fundamentally different. We have shown that both the universal and range infection functions can lead to regular, deterministic cycles when there are costs. For the universal function this leads to fluctuations in the transmission rate, while for the range function the fluctuations are between pure generalists and pure specialists. However, when there is a matching function we found that stable deterministic cycles do not exist. Instead we have shown that oscillations occur driven by the inherent incompatibility of the optimal host and parasite strategies. This result is in accordance with models of matching alleles in continuous time, which have shown only damped cycles rather than deterministic stable limit cycles [43,49]. This result also relates to the idea of 'stochastic persistence' [50], since regular input of mutations (i.e. faster than a full separation of ecological and evolutionary timescales) is essential for the cycles to be sustained. There are a number of implications to these different types of cycles. The deterministic cycles generated by the universal and range models are more regular and consistent, making their behavior more predictable. In contrast, the stochastic oscillations of the matching interaction tend to be irregular and vary in period and amplitude, making their behavior unpredictable. Stochastic fluctuations may also be less robust to changes in assumptions about mutation and standing variation. Distinguishing between these two forms of cycles empirically would be challenging due to environmental variation, but if FSD can be observed over multiple cycles, evidence of regularity could be looked for. An exciting question that thus emerges is whether the inherent differences among the fluctuating dynamics observed across infection interactions might support

different levels of genetic diversity within and among populations. It is yet unclear whether cycles generated under a specialist-generalist continuum (i.e. range or gene-for-gene) framework can be considered equivalent to those generated under a purely specialist (i.e. matching) framework.

By including explicit ecological dynamics in our models we have been able to assess how host and parasite life-history characteristics impact the potential for FSD. We have found that, no matter the infection function, cycles are most likely when hosts are long-lived and exist at high, but not the highest, densities. These results suggest that cycles are promoted when encounter rates are reasonably high. When encounter rates are low, so too is the potential for infection; therefore selection for costly host resistance is likely to be limited. At the other extreme, if encounter rates are very high then there will be considerable selection for resistance leading to an 'arms race dynamic' (ARD). It is in between these two extremes when cycles are most likely to occur. These results emphasise the role ecology plays in driving FSD in our models, since cycles only arise for certain regions of parameter space. Empirical studies in bacteria-phage systems agree with the predictions from our models, with environmental conditions that increase host-parasite encounter rates causing a shift from FSD to ARD [26-28]. This pattern is consistently seen in the stochastic oscillations from the matching model as well as the stable cycles of the universal and range models, suggesting this parameter dependency is robust.

Our models have demonstrated that there are a wide range of interactions between hosts and parasites that can lead to fluctuating selection. We require that

there are costs to resistance and infectivity to produce deterministic cycles in range or universal models, consistent with previous theory showing that costs are necessary but not sufficient for FSD to occur in gene-for-gene systems [3]. However, highly specific matching interactions produce stochastic oscillations. Our models are novel in that they demonstrate that specificity is not required for fluctuating selection to occur. Both the host life-history and the disease characteristics that promote FSD are consistent across all the different infection interactions. We can therefore make robust predictions for the types of host-parasite interactions that are most likely to lead to coevolutionary cycles. We note that the timescale of the cycles seen in our models is somewhat slower than those seen in classic gene-for-gene or matching-allele models. This is because we assume a separation of ecological and evolutionary timescales, whereas the genetic models are essentially at an ecological timescale with multiple competing strains. The cycles considered here are purely at the evolutionary timescale, with the population dynamics always being at, or close to (in simulations), an equilibrium. We also note that our methods assume a large number of loci with small additive effects, as opposed to classic population genetics models, which generally assume a small number of loci and epistasis between them. Future work will address when the discreteness that arises from a smaller number of loci has a significant effect on the results, but without a detailed understanding of the genetic basis of a particular interaction the quantitative assumption gives general insights.

Empirical evidence from a number of host-parasite systems indicates that fluctuating selection is a common form of coevolutionary dynamics. Several

studies have reported indirect evidence of FSD (or host-parasite relationships capable of FSD) based on phylogenetic data (e.g. *Arabidopsis* plants and *Pseudomonas* bacteria [51]), highly specific genetic interactions (e.g. sticklebacks and trematodes [52]), or high levels of polymorphism in immune genes (e.g. in the vertebrate Major Histocompatibility Complex [53]). Direct evidence of FSD primarily comes from time-shift experiments [54] between crustaceans and bacteria [55], water snails and trematodes [56], and bacteria and phages [26-28; 57]. The predictions from our models therefore have wide relevance within coevolutionary host-parasite systems. Given the ubiquity of ecological feedbacks and the diversity of different infection interactions our work emphasizes the considerable potential for host-parasite coevolution to generate fluctuating selection.

Author Contributions

ABe conceived of and designed the study, carried out the mathematical modeling and simulations, and drafted the manuscript. BA carried out mathematical modeling and simulations, and helped draft the manuscript. AW helped design the study and helped draft the manuscript. RB helped carry out the mathematical modelling and helped draft the manuscript. ABu helped design the study and helped draft the manuscript. BK helped design the study and helped draft the manuscript. MB conceived of and designed the study and drafted the manuscript.

Acknowledgements

We thank two anonymous reviewers for their comments on an earlier version of this manuscript.

Ethics

No ethics approval was needed for this study.

Funding

Alex Best was funded by a Leverhulme Early Career Fellowship, and this work was supported by NERC grants NE/J009784/1 and NE/N014979/1.

Data Accessibility

No data is used in this study. C++ code used for the simulations can be found in the supplementary material.

Competing Interests

We have no competing interests.

References

1. van Baalen, M. (1998). Coevolution of recovery ability and virulence. *Proc R. Soc. B.*, 265(1393):317–325.
2. Best, A., White, A. and Boots, M.. (2009). The Implications of Coevolutionary Dynamics to Host-Parasite Interactions. *American Naturalist* 173:779-791.
3. Tellier, A. and J. K. M. Brown (2007). Stability of genetic polymorphism in host-parasite interactions. *Proc R. Soc. B.*, 274:809–817.
4. Best, A., A. White, E. Kisdi, J. Antonovics, M. A. Brockhurst, and M. Boots. (2010). The Evolution of Host-Parasite Range. *American Naturalist* 176:63-71.
5. M. Boots, A. White, A. Best, and R. G. Bowers (2014). How specificity and epidemiology drive the coevolution of static trait diversity in hosts and parasites. *Evolution*, 68:1594-1606.
6. Gandon, S., Buckling, A., Decaestecker, E. and Day, T. (2008). Host-parasite coevolution and patterns of adaptation across time and space. *J. Evol. Biol.*, 21:1861-1866.
7. Flor, H.H. (1956). The complementary genetic systems in flax and flax rust. *Adv. Genet.*, 8:29-54.
8. Jayakar, S. (1970). A mathematical model for interaction of gene frequencies in a parasite and its host. *Theor Pop Biol.*, 1:140-164.
9. Sasaki, A. (2000). Host-parasite coevolution in a multilocus gene-for-gene system. *Proc R. Soc. B.* 267:2183-2188.
10. Agrawal, A. and C. M. Lively. (2002). Infection genetics: gene-for-gene versus matching-alleles models and all points in between. *Evolutionary Ecology Research* 4:79-90.

11. Ashby, B. and Boots, M. (2017). Multi-mode fluctuating selection in host-parasite coevolution. *Ecology Letters*, 20:357-365.
12. Hall, A., Scanlan, P., Morgan, A. and Buckling, A. (2011). Host-parasite coevolutionary arms races give way to fluctuating selection. *Ecology Letters*, 14:635-642.
13. Clarke, B. (1979). Evolution of genetic diversity. *Proc Roy Soc. B.*, 205:453-474.
14. Hamilton, W. D. (1980). Sex versus non-sex versus parasite. *Oikos*, 35: 282-290.
15. Lively, C. (2009). The maintenance of sex: host-parasite coevolution with density-dependent virulence. *J. Evol. Biol.*, 22:2086-2093.
16. Lively, C. (2010). An epidemiological model of host-parasite coevolution and sex. *J. Evol. Biol.*, 23:1490-1497.
17. Lively, C. (1999). Migration, virulence and the geographic mosaic of adaptation by parasites. *Am. Nat.*, 153:S34-S47.
18. Gandon, S. (2002). Local adaptation and the geometry of host-parasite coevolution. *Ecology Letters*, 5: 246-256.
19. Morgan, A., Gandon, S. and Buckling, A. (2005). The effect of migration on local adaptation in a coevolving host-parasite system. *Nature*, 437:253-256.
20. Frank, S. A. (1993). Coevolutionary genetics of plants and pathogens. *Evol. Ecol.* 7:45-75.
21. S. A. Frank (1994). Coevolutionary genetics of hosts and parasites with quantitative inheritance. *Evol. Ecol*. 8:74–94.

22. Hamilton, WD (1993). Haploid dynamic polymorphism in a host with matching parasites – effects of mutation subdivision, linkage and patterns of selection. *J. Heredity*, 84:328-338.
23. Thrall, P and Burdon, J. (2003). Evolution of virulence in a plant host-pathogen metapopulation. *Science*, 299:1735-1737.
24. Scanlan, P., Hall, A., Lopez-Pascua, L, et al. (2011). Genetic basis of infectivity evolution in bacteriophage. *Mol. Ecol.*, 20:981-989.
25. Luijckx, P., Fienberg, H., Duneau, D. et al. (2013). A matching allele model explains host resistance to parasites. *Curr. Biol.,* 23:1085-1088.
26. Gomez, P. and A. Buckling (2011). Bacteria-phage antgaonistic coevolution in soil. *Science*, 332:106–109.
27. Lopez-Pascua, L., A. Hall, A. Best, A. D. Morgan, M. Boots, and A. Buckling (2014). Higher resources decrease fluctuating selection during host-parasite coevolution. *Ecology Letters*, 17:1380–1388.
28. Gomez, P., Ashby, B. and Buckling, A. (2015). Population mixing promotes arms race host-parasite coevolution. *Proc. Roy. Soc. B.*, 282:20142297.
29. Gandon, S., P. Agnew, and Y. Michalakis (2002). Coevolution between parasite virulence and host life-history traits. *American Naturalist*, 160(3):374–388.
30. Dieckmann, U. and R. Law (1996). The dynamical theory of coevolution: a derivation from stochastic ecological processes. *Journal of Mathematical Biology*, 34(5-6):579–612.
31. Marrow, P., U. Dieckmann, and R. Law (1996). Evolutionary dynamics of predator-prey systems: an ecological perspective. *Journal of Mathematical Biology*, 34:556–578.

32. Metz, J.A.J., S. A. H. Geritz, G. Mesz ena, F. J. A. Jacobs, and J. S. Van Heerwaarden (1996). Adaptive dynamics: a geometrical study of the consequences of nearly faithful reproduction. In S. J. van Strein and S. M. Verduyn Lunel, editors, *Stochastic and Spatial Structures of Dynamical Systems*, pages 183– 231. Elsevier: North-Holland.
33. Geritz, S. A. H., E. Kisdi, G. Meszena, and J. A. J. Metz. (1998). Evolutionarily singular strategies and the adaptive growth and branching of the evolutionary tree. *Evolutionary Ecology* 12:35-57.
34. Anderson, R. M. and R. M. May (1979). Population biology of infectious diseases: Part I. *Nature*, 280:361–367.
35. Kuznetsov, Y.. *Elements of Applied Bifurcation Theory*. Springer, 1995.
36. Kisdi E., Geritz, S. and Boldin, B. (2013). Evolution of pathogen virulence under selective predation: a construction method to fins eco-evolutionary cycles. *J. Theor. Biol.* 339:140-150.
37. Doedel, E. J. and B. E. Oldeman. *AUTO-07P: Continuation and bifurcation software for ordinary differential equations*. Technical report, Concordia University, Montreal, Canada, 2009.
38. May, R. M. and Anderson, R. M. (1983). Epidemiology and genetics in the coevolution of parasites and hosts. *Proc. R. Soc. B.*, 219:281-313.
39. Tellier, A. and Brown, J. (2008). The relationship of host-mediated induced resistance to polymorphism in gene-for-gene relationships. *Phytopathology*, 98:128-136.
40. Gandon, S. and Day, T. (2009). Evolutionary epidemiology and the dynamics of adaptation. *Evolution*, 826-838.

41. Quigley, B. Z., Garcia Lopez, D., Buckling, A. *et al.* (2012). The mode of host-parasite interaction shapes coevolutionary dynamics and the fate of host cooperation. *Proc R. Soc. B.,* 279:3742-3748.
42. Gokhale, C., Papkou, A., Traulsen, A. and Schulenburg, H. (2013). Lotka–Volterra dynamics kills the Red Queen: population size fluctuations and associated stochasticity dramatically change host-parasite coevolution. *BMC Evol. Biol.*, 13:254.
43. Ashby, B. and Gupta, S. (2014). Parasitic castration promotes coevolutionary cycling but also imposes a cost on sex. *Evolution*, 68:2234-2244.
44. Ashby, B., Gupta, S. and Buckling, A. (2014). Effects of epistasis on infectivity range during host-parasite coevolution. *Evolution*, 68:2972-2982.
45. Marrow, P., R. Law, and C. Cannings. (1992). The coevolution of predator-prey interactions: ESSs and Red Queen dynamics. *Proc R. Soc. B.*, 250:133–141.
46. Gandon, S., Buckling, A., Decaestecker, E. and Day, T. (2008). Host-parasite coevolution and patterns of adaptation across time and space. *J. Evol. Biol.*, 21:1861-1866.
47. Doebeli, M. (1996). Quantitative genetics and population dynamics. *Evolution*, 50:532-546.
48. Otto, S. and Nuismer, S. (2004). Species interactions and the evolution of sex. *Science*, 304:1018-1020.

49. Kouyos, R., Aslathe, M. and Bonhoeffer, S. (2007). The Red Queen and the persistence of linkage-disequilibrium oscillations in finite and infinite populations. *BMC Evol. Biol.*, 7:211.

50. Allen, J. (1975). Mathematical models of species interactions in time and space. *Am. Nat.*, 967:319-342.

51. Stahl, E., Dwyer, G., Mauricio, R. et al. (1999). Dynamics of disease resistance polymorphism at the Rpm1 locus of Arabidopsis. *Nature*, 400:667-671.

52. Rauch, G., Kalbe, M., and Reusch, T. (2006). One day is enough: rapid and specific host-parasite interactions in a stickleback-trematode system. *Biology Letters*, 2:382-384.

53. Penman, B., Ashby, B. Buckee, C. et al. (2013). Pathogen selection drives nonoverlapping associations between HLA loci. *Proc Nat. Acad. Sci.*, 110:19645-19650.

54. Gaba, S. and Ebert, D. (2009). Time-shift experiments as a tool to study antagonistic evolution. *Trends in Ecol. Evol.*, 24:226-232.

55. Decaestecker, E., Gaba, S., Raeymaekers, J. et al. (2007). Host-parasite 'Red Queen' dynamics archived in pond sediment. *Nature*, 450:870-U16.

56. Koskella, B. and Lively, C. (2007). Advice of the rose: experimental coevolution of a trematode parasite and its snail host. *Evolution*, 61:152-159.

57. Koskella, B. (2014). Bacteria-phage interactions across time and space: merging local adaptation and time-shift experiments to understand phage evolution. *Am Nat*, 184:S9-S21

Figure Legends

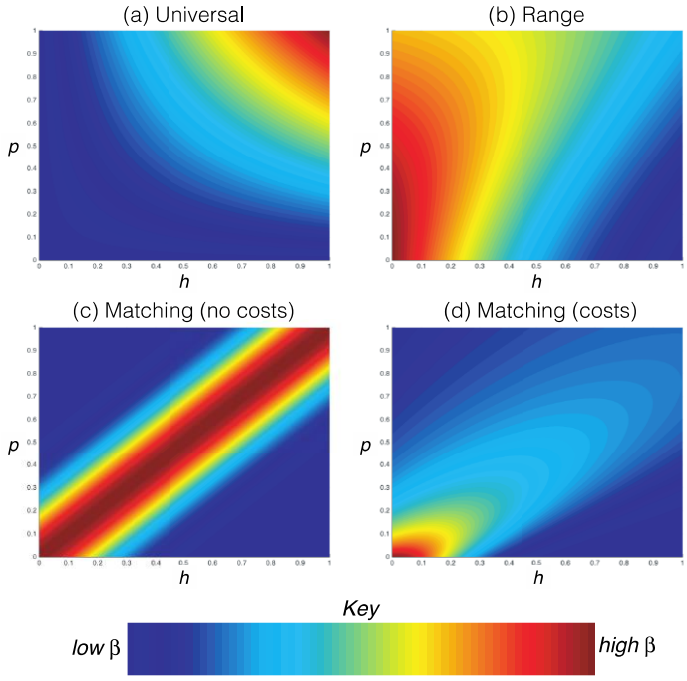

Figure 1

Heat maps showing the level of transmission, β, of parasite strains, p, against host strains, h, for our key infection functions: (a) Universal, (b) Range, (c) Matching without costs and (d) Matching with costs. The key shows that red indicates the highest transmission and blue the lowest transmission. Horizontal slices through these plots, showing β as a function of h for particular values of p, can be found in figure S1 in the SI. The exact forms are: (a) $\beta(h,p) = hp + 0.5$, (b) $\beta(h,p) = \beta_0(p)(1 - 1/(1 + \exp(3(p-h)))$ with $\beta_0(p) = 0.3 + 0.5(1 - p)/(1 + 1.45p)$, (c) $\beta(h,p) = \exp(-(p-h)^2/0.25^2)$, (d) $\beta(h,p) = \beta_0(p)(\exp(-(p-h)^2/(0.8p + 0.25)^2)$ with $\beta_0(p) = 15 - 12p/(1 + 0.85(p-1))$. We note that the explicit form of our trade-offs link maximum and minimum trait values through a smooth, polynomial-like curve where the second-derivative has constant sign (i.e. no inflections).

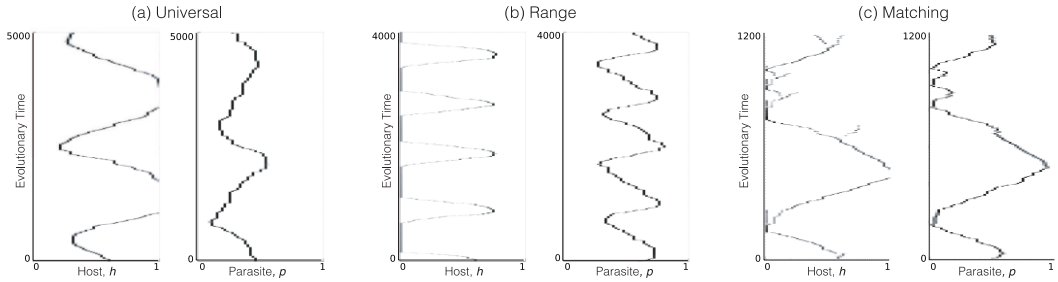

Figure 2

Output from numerical simulations showing the investment in host defence, h, and parasite infectivity, p, over evolutionary time using the three infections functions from figure 1: (a) Universal, (b) Range, (c) Matching. Simulations were conducted as described in the SI. In (a) $q = 0.1, b = 1, f = 0, \alpha_c = 5, \gamma = 0.1$, in (b) $q = 0.2, b = 1, f = 0, \alpha = 9, \gamma = 0.001$ and in (c) $q = 0.1, b = 1, f = 0, \alpha = 9\ \gamma = 0.1$. The parasite trade-off in (a) is $\alpha(p) = \alpha_c + 0.67 + 6.67p/(1 - 0.001(1 - p))$ and in (b) and (c) as given in figure 1. The host trade-offs are (a) $a(h) = 7.77 + 4.51h/(1 + 0.04(1 - h))$, (b) $a(h) = 55 + 45(1 - h)/(1 + 0.13h)$, (c) $a(h) = 30 - 20h/(1 + 0.2(h - 1))$. We note that these trade-offs are not subject to the assumptions made when proving the existence of the Hopf bifurcation in the SI (indeed if we chose trade-offs that satisfied those conditions, we would not see cycles in the simulations).

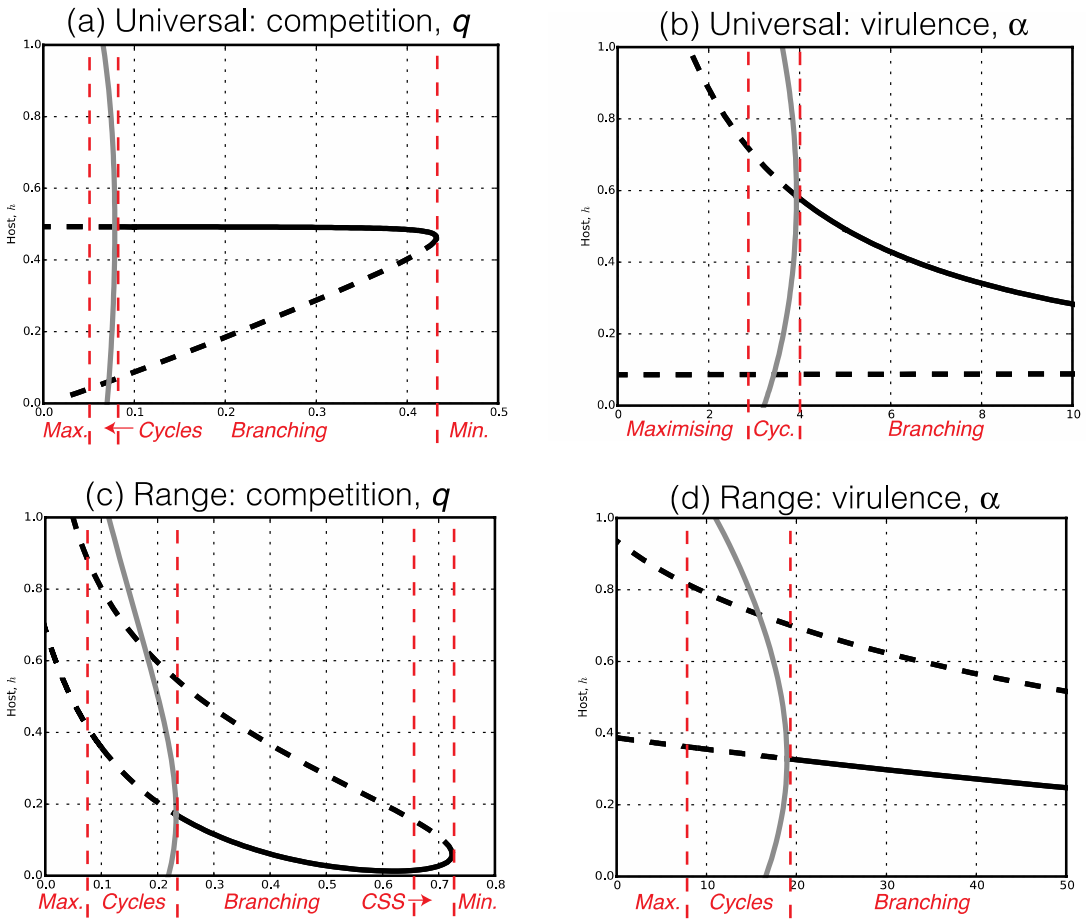

Figure 3

Bifurcation diagrams for (top row) the universal and (bottom row) range models showing the change in behavior at the singular point as we vary: (a), (c) competition, q, and (b), (d) virulence, α, in terms of host investment, h. Solid black lines denote convergence stable singular points, dashed black lines non-convergence stable singular points (i.e. repellers) and solid gray lines the upper and lower limits of a coevolutionary cycle. The red vertical dashed lines separate regions of behavior as annotated along the bottom of the plots. The *Maximize* and *Minimize* labels refer to the host's behaviour. In these regions the parasite either displays the same behavior or reaches a CSS. Default parameter values are: $q = 0.1, b = 1, f = 0$ with (a) and (b) $\alpha_c = 5, \gamma = 0.1$, and (c) and (d) $\alpha = 9, \gamma = 0.001$ with the trade-offs as given in figures 1 and 2. Again, we note that these

trade-offs are not subject to the assumptions made when proving the existence of the Hopf bifurcation

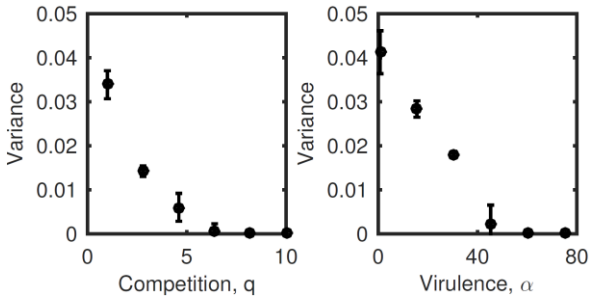

Figure 4

Plots showing the variance in the host trait over the final 20% of numerical simulations, using the matching model for (a) competition, q, and (b) virulence, α. A larger variance indicates larger cycles. Zero variance occurs where there is parasite extinction. Parameter values are as of figure 2.

Supplementary Information

A. Detailed description of analytic methods and results

A1. Model and methods

As stated in the main text, we base the host-parasite population dynamics on a classic SIS model as follows:

(S1) $\frac{dS}{dt} = (a - q(S + I))(S + fI) - bS - \beta SI + \gamma I$

(S2) $\frac{dI}{dt} = \beta SI - (b + \alpha + \gamma)I$.

with the parameters as described in the main text. *For consistency, in this SI we refer to the equation numbers from within this document, and not to those in the main text.* The methods used below not only build on classic adaptive dynamics theory (Metz et al., 1996; Marrow et al., 1996; Dieckmann & Law, 1996; Geritz et al., 1998) but also the related tools of critical function analysis (de Mazancourt & Dieckmann, 2004; Bowers et al., 2005; Kisdi, 2006) and, in particular, a recent study focussed on finding cycles between parasite virulence and predator densities (Kisdi et al., 2013).

Using the adaptive dynamics framework to consider evolution, the success or otherwise of an invading mutant depends on its invasion fitness, given by its exponential growth rate when rare (Metz et al., 1996; Geritz et al., 1998). For a mutant host we can calculate this from the dominant eigenvalue of the mutant equations' Jacobian as,

(S3) $s(\bar{h}; h, p) = \lambda_+ = \frac{T}{2} + \sqrt{T^2 - 4D}/2$

where,

(S3) $T = a(\bar{h}) - q(\hat{S} + \hat{I}) - 2b - \beta(\bar{h}, p)\hat{I} - \alpha(p) - \gamma$

(S4) $D = [a(\bar{h}) - q(\hat{S} + \hat{I}) - b - \beta(\bar{h}, p)\hat{I}][-b - \alpha - \gamma]$
$-[\gamma + f(a(\bar{h}) - q(\hat{S} + \hat{I}))]\beta(\bar{h}, p)\hat{I}$

and here (and below), $\hat{I}$ and $\hat{S}$ represent the steady state values at the resident equilibrium. We note, as stated in the main text, that in the case f=0, $g = 0$ this simplifies to,

(S6) $s(\bar{h}; h, p) = a(\bar{h}) - q(\hat{S} + \hat{I}) - b - \beta(\bar{h}, p)\hat{I}$

and we will use this expression from here on in our algebraic analysis. For the parasite we can derive its fitness from the growth rate of a mutant in the infected class as,

(S7) $r(\bar{p}; h, p) = \beta(h, \bar{p})\hat{S} - b - \alpha(\bar{p}) - \gamma.$

Assuming f=0, $g = 0$, the coevolutionary dynamics are described by,

(S8) $\frac{dh}{dt} = \varphi^h S \frac{\partial s}{\partial \bar{h}}\Big|_{\bar{h}=h} = \varphi^h \hat{S}[a_{\bar{h}} - \beta_{\bar{h}}\hat{I}]$

(S9) $\frac{dp}{dt} = \varphi^p \left.\frac{\partial r}{\partial \bar{p}}\right|_{\bar{p}=p} = \varphi^p \hat{I}[\beta_{\bar{p}}\hat{S} - \alpha_{\bar{p}}]$

where subscripts denote derivatives and φ^h and φ^p controls the respective speed of evolution between host and parasite (which is the product of the mutation rate and variance and a factor of 1/2). We will assume throughout that $\varphi^h = \varphi^p = 1$ to simplify parts of the analysis.

Coevolution will continue until either the two selection gradients are simultaneously zero (i.e. there is no longer directional selection on either species) and a coevolutionary 'singular point' has been reached (h^*,p^*), or until a maximum or minimum trait has been reached (due to physiological constraints in the host or parasite – note that at such point the fitness gradients are not necessarily zero but further evolution in one direction is prevented), or it may continually cycle. At a singular point, the coevolutionary behavior depends on a number of second-order properties (see Geritz et al., 1998). The point is *evolutionarily stable* (ES) if nearby mutants cannot invade the resident strategy; it is *convergence stable* (CS) if the point is locally attracting; and it is *mutually invadable* (MI) if both mutant and resident strains have positive invasion fitness. ES is given by the second-order term, for example in the host,

(S10) $\left.\frac{\partial^2 s}{\partial \bar{h}^2}\right|_{\bar{h}=h=h^*} < 0$

while convergence stability for a coevolutionary model is determined by the 2x2 Jacobian (Marrow et al., 1996),

(S11) $J = \begin{pmatrix} \varphi^h \hat{S}\left[\frac{\partial^2 s}{\partial \bar{h}^2} + \frac{\partial^2 s}{\partial \bar{h} \partial h}\right] & \varphi^h \hat{S} \frac{\partial^2 s}{\partial \bar{h} \partial p} \\ \varphi^p \hat{I} \frac{\partial^2 r}{\partial h \partial \bar{p}} & \varphi^p \hat{I}\left[\frac{\partial^2 r}{\partial \bar{p}^2} + \frac{\partial^2 r}{\partial \bar{p} \partial p}\right] \end{pmatrix}$

evaluated at the singularity, and mutual invadibility by the mixed derivative, for example in the host,

(S12) $\frac{\partial^2 s}{\partial \bar{h} \partial h}\Big|_{\bar{h}=h=h^*} < 0$

The four cases of particular interest, as described in the main text are: a *Continuously Stable Strategy* (ES and CS), an *evolutionary branching point* (CS and MI but not ES), *coevolutionary cycles* (loss of CS through a supercritical Hopf bifurcation), and *maximisation/minimisation* of one or both species to bounds of evolution (non-CS but not cycling).

The key infection functions we use are shown in figure 1 in the main text. In figure S1 we also show these functions as 'snapshots' of infection for specific parasite types against all hosts. To recap, the general forms are:

i) Universal:

(S13) $\beta(h,p) = \sigma(h)\rho(p) + k$

ii) Range:

(S14) $\beta(h,p) = \beta_0(p)\left(1 - \frac{1}{1+\exp(\kappa(p-h))}\right)$

iii) Matching:

(S15) $\beta(h,p) = \beta_0(p)exp\left(-\left(\frac{p-h}{\eta p+c}\right)^2\right)$

A2. Results

No costs

We first consider the case where both the host and parasite can evolve to change the transmission term without incurring costs. Without costs to either the host or parasite (including both forms of parasite trade-off considered here) the respective fitness gradients found using equations (S8) and (S9) are given by

(S16) $\frac{\partial s}{\partial \bar{h}}\Big|_{\bar{h}=h} = -\beta_{\bar{h}}\hat{I}$

(S17) $\frac{\partial r}{\partial \bar{p}}\Big|_{\bar{p}=p} = \beta_{\bar{p}}\hat{S}$

Therefore a coevolutionary singular point can only exist if $b_{\bar{h}} = b_{\bar{p}} = 0$. By definition this can never be true for a Universal or Range function (since $\beta_h \neq 0$ in both cases) and would only be true for the specific Matching function when $h=p$ and $b_0(p) = b_0$ is a constant (e.g. figures 1c, S1c). In fact, in this case there will be a continuum of such singular points, none of which is convergence stable. Under the full assumptions of adaptive dynamics, this will lead to a random walk through trait space. However, if we assume that there is not a complete separation of timescales such that new mutations can appear before the system has reached its dynamic attractor, cyclic behavior will be seen due to the 'trail' of strains on one side of the current resident. An example of these '*stochastic cycles*' from simulations of the coevolutionary process can be found in Boots et al., 2014.

With costs

Here we initially show that any generic infection function, including all three of our example cases, may yield a Hopf bifurcation (a critical point where a system's stability switches from an equilibrium to a limit cycle) when there are costs to resistance and/or infectivity. We consider the convergence stability of the singular point where the two fitness gradients (S8) and (S9) are simultaneously zero. This is governed by the eigenvalues of the Jacobian, J, of the system (Marrow et al., 1996 and see above),

$$\text{(S18) } J = \begin{pmatrix} \hat{S}[a_{\bar{h}\bar{h}} - \beta_{\bar{h}\bar{h}}\hat{I} - \beta_{\bar{h}}\hat{I}_h] & \hat{S}[-\beta_{\bar{h}p}\hat{I} - \beta_{\bar{h}}\hat{I}_p] \\ \hat{I}[\beta_{h\bar{p}}\hat{S} + \beta_{\bar{p}}\hat{S}_h] & \hat{I}[\beta_{\bar{p}\bar{p}}\hat{S} - \alpha_{\bar{p}\bar{p}} + \beta_{\bar{p}}\hat{S}_p] \end{pmatrix}$$

where subscripts denote derivatives, and hereafter evaluation at the singular point is intended but not made explicit. Let us for now assume that there is no simple decomposition of $\beta(h,p)$. The characteristic equation of this Jacobian reveals that the eigenvalues of the singular point are,

$$\text{(S19) } \lambda = \frac{B}{2} \pm \frac{\sqrt{B^2-4C}}{2}$$

where

$$\text{(S20) } B = tr(J) = \hat{S}\left[a_{\bar{h}\bar{h}} - \beta_{\bar{h}\bar{h}}\hat{I} - \beta_{\bar{h}}\hat{I}_h\right] + \hat{I}[\beta_{\bar{p}\bar{p}}\hat{S} - \alpha_{\bar{p}\bar{p}} + \beta_{\bar{p}}\hat{S}_p]$$

$$\text{(S21) } C = \det(J) = \hat{S}\hat{I}\left(\left[a_{\bar{h}\bar{h}} - \beta_{\bar{h}\bar{h}}\hat{I} - \beta_{\bar{h}}\hat{I}_h\right]\left[\beta_{\bar{p}\bar{p}}\hat{S} - \alpha_{\bar{p}\bar{p}} + \beta_{\bar{p}}\hat{S}_p\right] + [\beta_{\bar{h}p}\hat{I} +\right.$$

$\beta_{\bar{h}}\hat{I}_p][\beta_{h\bar{p}}\hat{S} + \beta_{\bar{p}}\hat{S}_h]\big)$

For a Hopf bifurcation to occur, the two eigenvalues must have Im(λ) non-zero with Re(λ) simultaneously equal to zero; This occurs when B=0 and C>0. At this point we simply wish to show that parameters and trade-offs exist that produce a Hopf bifurcation. We can therefore fix our trade-offs to take certain forms. We shall explore how the potential for cycles depends on the trade-off shape later in the main text. In particular, no matter the sign of each of the derivatives in B, one or more of the trade-off curvatures can always be chosen such that B=0; for example $a_{\bar{h}\bar{h}} = \beta_{\bar{h}\bar{h}}\hat{I} + \beta_{\bar{h}}\hat{I}_h$; $\alpha_{\bar{p}\bar{p}} = \beta_{\bar{p}\bar{p}}\hat{S} + \beta_{\bar{p}}\hat{S}_p$ is a particularly useful choice, though clearly many other combinations exist that satisfy *B=0*. It therefore remains to show that $C > 0$ is possible in the neighbourhood of $B = 0$. Since from (S20) at $B = 0$ we have $\hat{I}\left[\beta_{\bar{p}\bar{p}}\hat{S} - \alpha_{\bar{p}\bar{p}} + \beta_{\bar{p}}S_p\right] = -\hat{S}\left[a_{\bar{h}\bar{h}} - \beta_{\bar{h}\bar{h}}\hat{I} - \beta_{\bar{h}}\hat{I}_h\right]$, we can now write,

(S22) $C = \hat{S}\hat{I}\left(-\frac{I}{S}\left[\beta_{\bar{p}\bar{p}}\hat{S} - \alpha_{\bar{p}\bar{p}} + \beta_{\bar{p}}\hat{S}_p\right]^2 + \left[\beta_{\bar{h}p}\hat{I} + \beta_{\bar{h}}\hat{I}_p\right]\left[\beta_{h\bar{p}}\hat{S} + \beta_{\bar{p}}\hat{S}_h\right]\right)$

Again, though, we can always choose curvatures that make the first term zero without jeopardising the value of $B = 0$; in particular our choice above of $a_{\bar{h}\bar{h}} = \beta_{\bar{h}\bar{h}}\hat{I} + \beta_{\bar{h}}I_h$; $\alpha_{\bar{p}\bar{p}} = \beta_{\bar{p}\bar{p}}\hat{S} + \beta_{\bar{p}}\hat{S}_p$ would satisfy both conditions. It therefore remains for us to show that

(S23) $C = \hat{S}\hat{I}\left[\beta_{\bar{h}p}\hat{I} + \beta_{\bar{h}}\hat{I}_p\right]\left[\beta_{h\bar{p}}\hat{S} + \beta_{\bar{p}}\hat{S}_h\right]>0$

is possible. By considering the derivatives of the S and I equilibrium densities (i.e. the solutions to (S1)-(S2)), and now explicitly assuming evaluation at the singular point, we find that (S23) becomes

(S24) $C = \hat{S}^2\hat{I}^2\left[\beta_{hp} - \frac{\beta_h\beta_p}{q+\beta}\right]\left[\beta_{hp} - \frac{\beta_h\beta_p}{\beta}\right] > 0$

Clearly for small q (low competition, meaning large population sizes) this condition will be satisfied. Thus we have established that, for suitable cost structures, there may be eigenvalues with zero real part and non-zero imaginary parts, indicating the existence of a Hopf bifurcation and the potential for cycles. It is important to note that this is the point at which cycles emerge. Once this point is passed through, further changes to the trade-offs or parameters will lead to the cycles growing in size (with the eigenvalues at the singular point being complex with positive real part). Thus, while the trade-off curvatures are required to obey certain conditions at the Hopf bifurcation, coevolutionary cycles will occur for a wider range of conditions (see §A3 and figure S5 of this SI). Moreover, maintaining the choice of curvature described above, if we choose the gradients and curvatures such that C=0, then we have zero trace and zero determinant of our Jacobian which corresponds to a Bogdanov-Takens point, a co-dimension two bifurcation which is the meeting of saddle-node and Hopf bifurcation curves (Kuznetsov, 1995, Kisdi et al., 2013). At such a point there necessarily emerges a homoclinic orbit, bounding the region of the cycles. In particular, once the cycles grow to such a size that they pass the homoclinic orbit, there will be no convergence stable singular points or stable coevolutionary cycles remaining in the system. The system would

therefore evolve to maximum or minimum investment by the host or parasite depending on the positioning of the nullclines. Also, the existence of the saddle-node bifurcation suggests parameter values exist where there are no singular points present.

We now apply the general condition we have calculated to each of the example infection functions we introduced in figure 1.

i) Universal

In the case of universal transmission with $\beta(h,p) = \sigma(h)\rho(p) + k$, we are able to further simplify the expression in equation (S24) since $\beta_{hp} = \sigma_h\rho_p$; $\beta_h = \sigma_h\rho$; $\beta_p = \sigma\rho_p$ (recall subscripts denote derivatives), meaning this becomes

$$\text{(S25) } C = \hat{S}^2\hat{I}^2\left[\sigma_h(h)\rho_p(p)\right]^2\left[\frac{k}{\sigma\rho+k}\right]\left[\frac{k+q}{\sigma\rho+k+q}\right] > 0$$

(assuming that our trade-off curvatures are such that B (S20) and the first term of C (S21) are both zero as described above). Wherever $k > 0$ (S25) is necessarily positive so cycles will always be possible. We see that in the special case that k=0 we have C=0 and there can be no cycles in the system. In fact, it can be shown that when k=0 the bottom-left entry in the Jacobian (S18) is necessarily zero, ensuring that there are no cycles even without making assumptions on the trade-offs as above. To show this we note that by differentiating at the population dynamics equilibrium we have $S_h = -\beta_h S/\beta$, meaning the bottom-left entry in (S18) becomes,

(S26) $\hat{I}[\beta_{hp}S - \beta_h\beta_p S/\beta]$.

Now substituting the general universal infection function $\beta = \sigma(h)\rho(p) + k$ and its derivatives in to (S26) we have,

(S27) $\hat{I}\left[\sigma_h\rho_p S - \frac{\sigma_h\rho_p\sigma(h)\rho(p)S}{\sigma(h)\rho(p)+k}\right]$,

which vanishes when k=0. Because of this we know that the eigenvalues must be real, hence there can be no cycling, irrespective of any assumptions on the trade-offs. We note that the interpretation of this entry being zero is that the host trait is having no impact on the parasite selection gradient.

(ii) Range

The condition for cycling in the range model reduces considerably compared to (S24) since $a(p) = a$ is a constant. This means not only do we know that $\alpha_{pp} = 0$, but also that at the singular point we must have $\beta_p = 0$ from (S9). As such, a choice of $\beta_{pp} = 0$ means that the bottom-right entry in the Jacobian (S18) is necessarily zero, and only a condition remains to be taken on the host's trade-off is required to let B=0. Additionally, substituting these zero values in to equation (S24), in particular noting again that $\beta_p = 0$, means that the condition for cycling reduces to,

(S28) $C = \hat{S}^2\hat{I}^2\beta_{hp}^2 > 0$

which is always true and so we confirm that a Hopf bifurcation may occur for any form of this infection function.

(iii) *Matching*

Here we again assume that virulence is not involved in the parasite trade-off. This means that the condition for cycling is identical to equation (S26) for range, which is always true so a Hopf bifurcation can occur for any form of this infection function. However, when analysing this model we found that the Hopf bifurcation is always *subcritical* meaning that the cycles that arise are unstable. The complexity of the model prevented us from proving this analytically, but we plotted bifurcation diagrams and conducted numerical simulations for a comprehensive range of parameters and found that this was always the case.

A3. Host and Parasite Trade-offs

When proving the existence of a Hopf bifurcation in the earlier section, we fixed our trade-offs such that the curvatures at the co-singular point took particular values. Here we explore how the potential for cycles depends on the trade-off shapes, and in particular show that cycles are not limited to a restrictive and/or unrealistic set of trade-offs. In figure S5 we show bifurcation diagrams as the parameter that controls the curvature in the respective trade-off functions (see figure legend) is varied for the universal model. We note that a value of zero gives a linear trade-off. It is clear from these diagrams that cycles occur for a reasonable range of near-linear trade-off shapes. In particular cycles occur for weakly decelerating trade-offs for both host and parasite. Similar results occur for the range model.

References found only in the SI

De Mazancourt, C. & Dieckmann, U. (2004). Trade-off geometries and frequency-dependent selection. *Am. Nat.*, 164:765-778.

Bowers, R., Hoyle, A., White, A. and Boots, M. (2005). The geometric theory of adaptive evolution: trade-off and invasion plots. *J. Theor. Biol*, 233:363-377.

Kisdi (2006). Trade-off geometries and the adaptive dynamics of two coevolving species. *Evol. Ecol. Res.*, 8:959-973.

B. Numerical simulation methods

The simulation code used is available as a supplementary file. The simulations were conducted in the C++ programming language. Arrays of N=50 host ($h=0:1$) and parasite ($p=0:1$) types were initialised, and the densities of all but one host and parasite type set to 0. The following algorithm then applied in each evolutionary time-step:

- The population dynamics of all types were numerically solved using a 4^{th} order Runge-Kutta solver for a large enough number of steps (8000) that the system is nearby its dynamic attractor.
- Any types whose density was below a low threshold of 0.005 were assumed extinct and their densities set to 0.
- A new (mutant) host or parasite type was generated one strain 'up' or 'down' from a resident type. Often multiple strains would still be present as the population dynamics had not yet reached the dynamic attractor. In this case, the 'resident' (i.e. the strain producing the mutant) was chosen probabilistically based on the relative densities (i.e. if two strains were present at densities of 3 and 2 respectively, there would be a 60% chance of the first strain generating the mutant and a 40% chance of the second strain). The density of the mutant

strain was set at 10% of the resident (if the strain already had a positive density it was increased by this amount).

- The initial invasion success of the mutant was checked against a demographic stochasticity function (see Dieckmann & Law, 1996). This function causes extinction of mutant strains with negative or positive but small initial growth rates. With a probability inversely proportional to fitness (with negative fitness meaning 0 probability), that mutation event does not occur. This ensures that the relative speeds of evolution of the two coevolving species match with the analytical approach.

This evolutionary time-step algorithm was then repeated. The densities were recorded at the end of each run of the population dynamics.

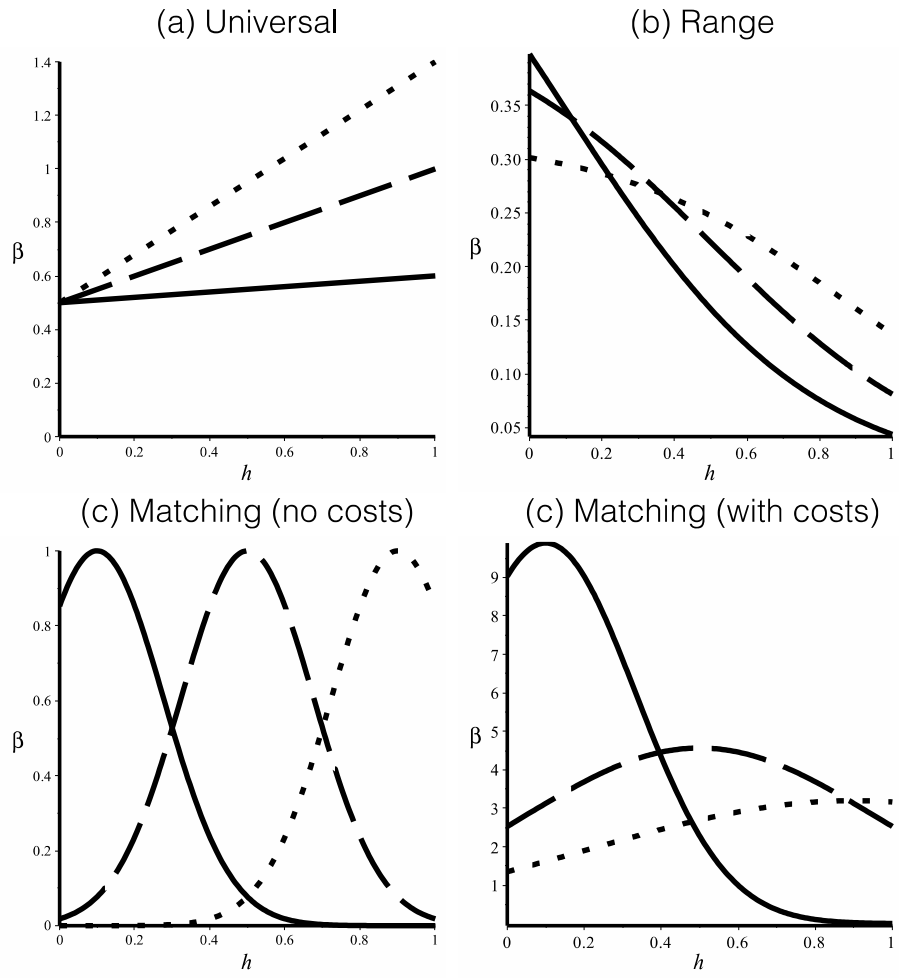

Figure S1

Plots showing snapshots of transmission, β, for specific parasite strains, p, (solid line is for *p=0.*1, dashed line *p=0.*5 and dotted line *p=0.*9) against all host strains, h, for (a) Universal, (b) Range, (c) Matching without costs and (d) Matching with costs. The exact forms are: (a) $\beta(h,p) = hp + 0.5$, (b) $\beta(h,p) = \beta_0(p)(1 - 1/(1+\exp(3(p-h)))$ with $\beta_0(p) = 0.3 + 0.5(1-p)/(1+1.45p)$, (c) $\beta(h,p) = \exp(-(p-h)^2/0.25^2)$, (d) $\beta(h,p) = \beta_0(p)(\exp(-(p-h)^2/(0.8p+0.25)^2)$ with $\beta_0(p) = 15 - 12p/(1+0.85(p-1))$.

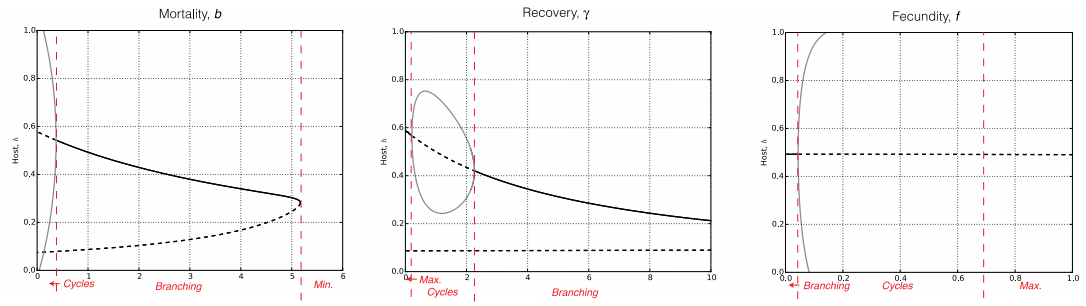

Figure S2

Bifurcation diagrams for the universal model showing the change in behavior at the singular point as we vary: (a), mortality, b, (b) recovery, γ, and (c) infected fecundity, f, in terms of host investment, h. Solid black lines denote convergence stable singular points, dashed black lines non-convergence stable singular points (i.e. repellers) and solid gray lines the upper and lower limits of a coevolutionary cycle. The red vertical dashed lines separate regions of behavior as annotated along the bottom of the plots. Default parameter values are as of figure 3 in the main text. (We note here that the general results are not restricted to assuming high levels of sterilization. Cycles in the universal model with our default parameters occur for intermediate levels of sterility (see panel (c)), but we found that they could still occur up to f=1 for other parameter sets (results not shown).)

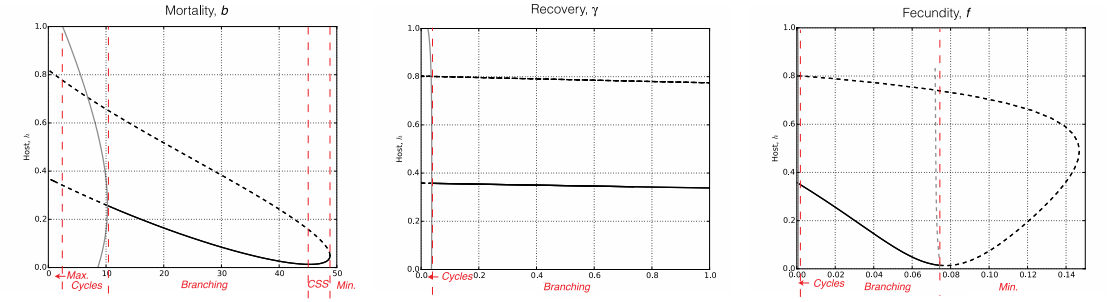

Figure S3

Bifurcation diagrams for the range model showing the change in behavior at the singular point as we vary: (a), mortality, b, (b) recovery, γ, and (c) infected fecundity, f, in terms of host investment, h. Solid black lines denote convergence stable singular points, dashed black lines non-convergence stable singular points (i.e. repellers) and solid gray lines the upper and lower limits of a coevolutionary cycle. The red vertical dashed lines separate regions of behavior as annotated along the bottom of the plots. Default parameter values are as of figure 2 in the main text.

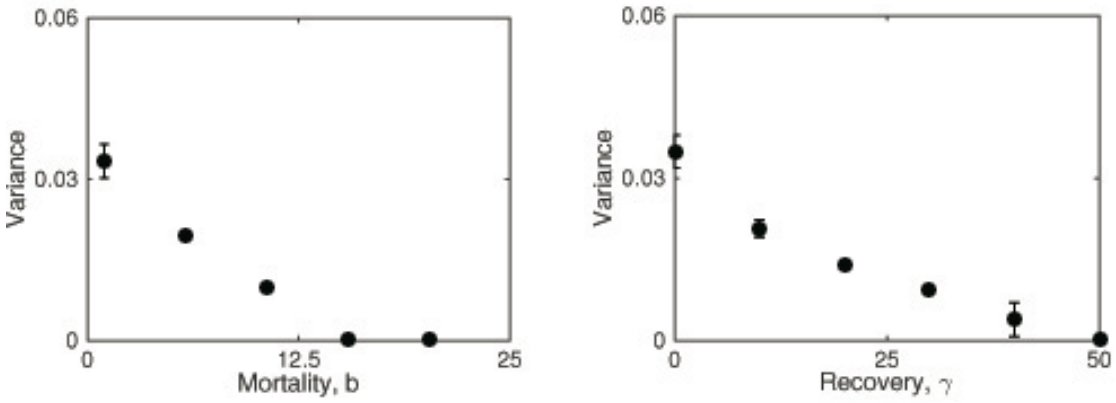

Figure S4

Plots showing the variance in the host trait over the final 20% of numerical simulations, using the matching model for (a) mortality, b, and (b) recovery, γ. A larger variance indicates larger cycles. Zero variance occurs where there is parasite extinction. Parameter values are as of figure 4 in the main text.

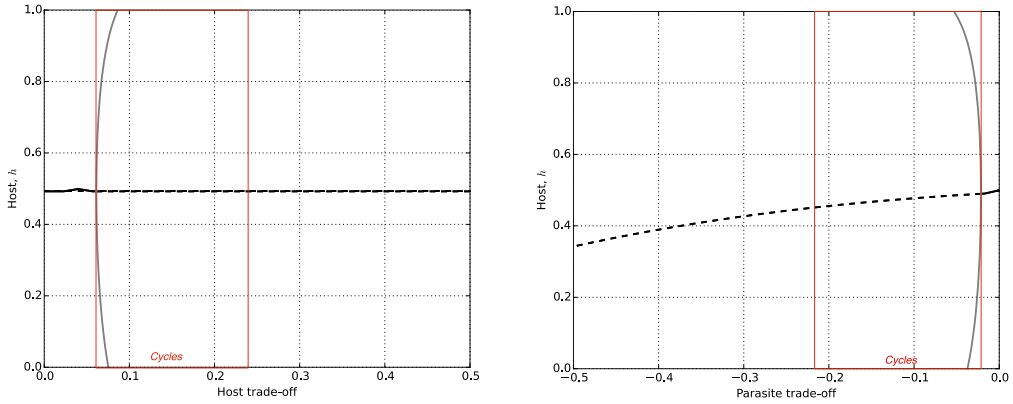

Figure S5

Bifurcation diagrams as (left) the host trade-off shape and (right) parasite trade-off shape are varied. The trade-offs used are $a(h) = 7.77 + 4.51h/(1 + \vartheta_h(1 - h))$ and $\alpha(p) = \alpha_c + 0.67 + 6.67p/(1 - \vartheta_p(1 - p))$, and it is the ϑ parameters which are varied. Solid black lines denote convergence stable singular points, dashed black lines non-convergence stable singular points (i.e. repellers) and solid gray lines the upper and lower limits of a coevolutionary cycle. The red vertical

dashed lines highlight the regions that generate cycles. Default parameter values are as of figure 3 in the main text.

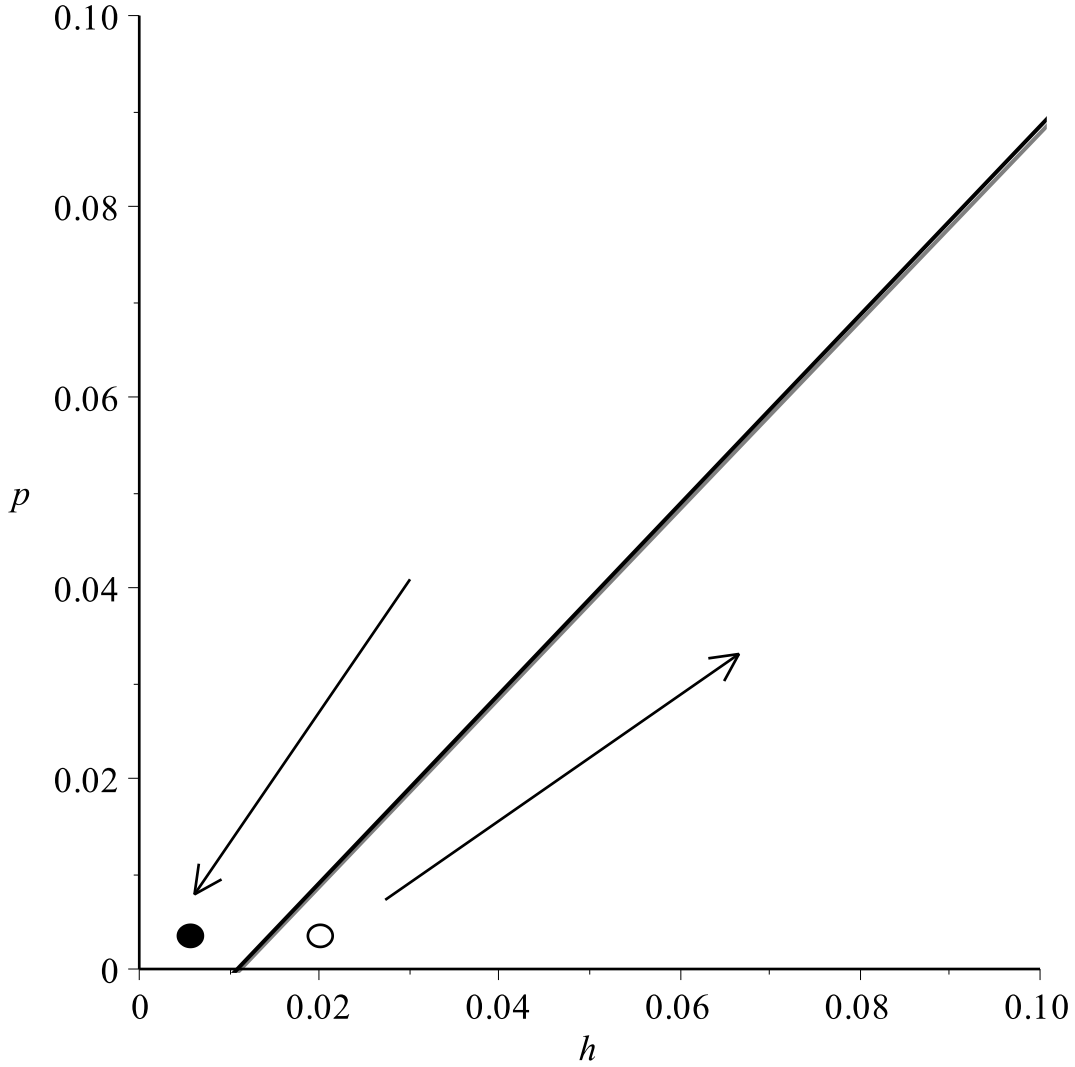

Figure S6

The deterministic adaptive dynamics for the matching model in the phase space of h and p. The host nullcline is shown in black and the parasite nullcline in gray. Above both nullclines selection is to reduce investment in both the host and parasite, which would lead to minimal investment. However, the nullclines are suitably close to the main diagonal that small mutations allow strains to appear below the nullclines, where selection is to increase investment.